Impact of glacial isostatic adjustment on zones of potential grounding line persistence in the Ross Sea Embayment (Antarctica) since the Last Glacial Maximum

Samuel T. Kodama[1], Tamara Pico[1], Alexander A. Robel[2], John Erich Christian[3], Natalya Gomez[4], Casey Vigilia[5], Evelyn Powell[6], Jessica Gagliardi[1], Slawek Tulaczyk[1], Terrence Blackburn[1]

[1]Earth and Planetary Science, University of California Santa Cruz, Santa Cruz, CA, USA

[2] School of Earth and Atmospheric Sciences, Georgia Institute of Technology, Atlanta, GA, USA

[3]Department of Geography, University of Oregon, Eugene, OR, USA

[4] Earth and Planetary Sciences, McGill University, Montréal, Québec, Canada

[5]Jackson School of Geosciences, University of Texas at Austin, Austin, TX, USA

[6] Lamont-Doherty Earth Observatory of Columbia University, Palisades, NY, USA

Correspondence to: Samuel T. Kodama (sakodama@ucsc.edu)

Abstract

Ice streams in the Ross Sea Embayment (West Antarctica) retreated up to 1,000 kilometers since the Last Glacial Maximum. One way that bathymetry influenced this retreat was through the presence of local bathymetric highs, or "pinning points", which decreased ice flux through the grounding line and slowed grounding line retreat. During this time, glacial isostatic adjustment vertically shifted the underlying bathymetry, altering the grounding line flux. Continental-scale modeling efforts have demonstrated how solid Earth-ice sheet interactions impact the deglacial retreat of marine ice sheets, however, these models are too coarse to resolve small-scale bathymetric features. We pair a high-resolution bathymetry model with a simple model of grounding line stability in an ensemble approach to predict zones of potential grounding line persistence in the Ross Sea Embayment for given combinations of surface mass balance rate, degree of ice shelf buttressing, basal friction coefficient, and bathymetry (corrected for glacial isostatic adjustment using three different ice sheet histories). We find that isostatic depression within the interior of the Ross Sea Embayment during the Last Glacial Maximum restricts zones where grounding lines can persist to near the edge of the continental shelf. ~~Grounding~~Most grounding lines cannot persist near the present-day grounding line until sufficient uplift has occurred (mid-Holocene; ~5 ka), and this uplift causes a net upstream migration of grounding line persistence zones across the deglaciation. Additionally, our results show that coarse resolution

31 bathymetry underpredicts possible stable grounding line positions, particularly near the present-
32 day grounding line, highlighting the importance of bathymetric resolution in capturing the impact
33 of glacial isostatic adjustment on ice stream stability.
34
35 **1. Introduction**
36   Since the Last Glacial Maximum (LGM) at approximately 26-19 ka (Clark et al., 2009), ice
37 streams in the Ross Sea Embayment sector of West Antarctica retreated up to 1,000 kilometers to
38 their present-day grounding line ~~positions (location~~ position (where ice transitions from grounded
39 to floating ~~to grounded~~). Bathymetry can influence the ~~retreat of~~ a marine ice sheets by guiding
40 grounding lines through deep submarine troughs (Halberstadt et al., 2016; Jones et al., 2021) or by
41 slowing retreat through local bathymetric highs known as "pinning points". Pinning points, either
42 a product of antecedent bathymetry or sediment deposited in the form of grounding zone wedges
43 (Bart et al., 2018; Bart and Tulaczyk, 2020; Jamieson et al., 2012; Simkins et al., 2018), can slow
44 or pause ice sheet retreat by decreasing ice flux through the grounding line (Jamieson et al., 2012;
45 Robel et al., 2022; Schoof, 2007).
46   Over the last deglaciation, the bathymetry underlying the marine-based (grounded below sea
47 level) Ross Sea Embayment of the Antarctic Ice Sheet has been modulated by glacial isostatic
48 adjustment (GIA), the solid Earth's response to ice sheet unloading through crustal deformation
49 and perturbations to the Earth's gravitational field and rotation axis (Kendall et al., 2005). Local
50 ice sheet retreat causes sea level to fall at the grounding line, due to solid-Earth rebound and a
51 decrease in gravitational attraction, which slows the modeled retreat rate for marine sectors of the
52 Antarctic Ice Sheet experiencing mass loss (de Boer et al., 2014; van Calcar et al., 2023; Gomez
53 et al., 2013, 2015, 2018; Konrad et al., 2015; Pollard et al., 2017). In the Ross Sea Embayment,
54 GIA-induced uplift is hypothesized to have stabilized the ice sheet during the Holocene by directly
55 triggering grounding line readvance to its present-day position (Kingslake et al., 2018), or by
56 modulating ice sheet sensitivity to ocean forcing, which similarly could have driven readvance
57 (e.g. Lowry et al., 2024).
58   Although coupled GIA-ice sheet models provide valuable insight into ice sheet-solid Earth
59 interactions across Antarctica, they are computationally expensive. As a result, ensemble runs of
60 ice sheet or coupled GIA-ice sheet models that can encompass uncertainties in climate and
61 glaciologic conditions are run at relatively coarse resolution (16-40 km; Albrecht et al., 2020, 2024;

62 van Calcar et al., 2023; Gomez et al., 2018; Pollard et al., 2017), and are unable to resolve smaller

63 scale bathymetric features, such as pinning points (≤5 km; e.g., McKenzie et al., 2023), which

64 influences grounding line evolution. Recent coupled GIA-ice sheet modeling showed that

65 increasing bathymetric resolution (from 2 km to 1 km) slowed ~~predictions of~~predicted grounding

66 line retreat by up to ~20% in the Amundsen Sea (Houriez et al., 2025); however such high-

67 resolution modeling is more appropriate for smaller regions (the Ross Sea Embayment is ~4x their

68 model domain size) and for timescales of centuries rather than millennia. Exploring the impact of

69 high-resolution bathymetry on grounding evolution since the LGM across a larger area, such as

70 the Ross Sea Embayment, is still a computational challenge.

71 Here, we use an ensemble ($n=9 \times 10^5$) of simple grounding line stability calculations to isolate

72 how bathymetric change due to GIA impacts ice stream grounding line persistence across the

73 deglaciation of the Ross Sea Embayment. We model possible grounding lines along 147 LGM ice

74 stream flowlines in the Ross Sea Embayment across high-resolution models of present-day and 20

75 ka GIA-corrected bathymetry. Rather than reconstructing an exact history of grounding-line

76 evolution, we predict zones where a potential grounding line could persist at 20 ka and present

77 day. This choice allows us to produce a probability distribution of locations where past ice stream

78 grounding lines were likely to persist, ~~which we term~~termed "zones of potential persistence",

79 across the entire Ross Sea Embayment. ~~We~~ We use these predictions to explore ~~the contribution~~

80 ~~of~~how GIA ~~to grounding line persistence at present-day and 20 ka grounding line locations,~~

81 ~~quantifying the impact of GIA on zones of potential persistence~~modulates ice stream stability

82 across the deglaciation.

2. Methods

2.1 Modeling Ross Sea Embayment Paleobathymetry

85 To reconstruct Ross Sea Embayment 20 ka bathymetry we modify present-day

86 BedMachine v1.38 bathymetry (500 m horizontal resolution; Morlighem et al., 2020) for the

87 spatiotemporal patterns of GIA caused by the deformational, gravitational, and rotational effects

88 associated with changes in ice load (i.e. ~~topography$_{20}$~~bathymetry$_{20\ ka}$ =

89 ~~topography$_{pres}$~~bathymetry$_{pres}$ – relative sea level$_{20\ ka}$)." Sedimentation would have also altered the

90 20 ka bathymetry of the Ross Sea Embayment since the LGM, however knowledge of the timing

91 and magnitude of sedimentation across the Ross Sea Embayment is limited to grounding zone

92 wedges (Bart et al., 2018; Danielson and Bart, 2024), and so we focus on the role of GIA. Our

Commented [SK1]: Is it okay if I change topography to bathymetry since we use bathymetry throughout the paper?

93   simulations are based on the sea-level theory and pseudo-spectral algorithm described by Kendall

94   et al. (2005), with a spherical harmonic truncation at degree and order 512 (spatial resolution of

95   ~40 km). This treatment includes the impact of load-induced Earth rotation changes on sea level

96   (Milne and Mitrovica, 1996), evolving shorelines, and the migration of grounded, marine-based

97   ice (Johnston, 1993; Kendall et al., 2005; Lambeck et al., 2003; Milne et al., 1999). Our GIA

98   simulations require two inputs: (1) an Earth structure model with a depth-varying viscosity of the

99   mantle along with an elastic lithospheric thickness; and (2) the space-time geometry of ice sheet

100   thickness. The resulting GIA output varies smoothly across spatial scales much broader than the

101   spatial scales of Ross Sea Embayment bathymetric changes.

102   The LGM extent and deglacial history of Antarctica is uncertain due to a paucity of datasets

103   constraining past ice thickness and sea-level change (Clark and Tarasov, 2014; Deschamps et al.,

104   2012; Golledge et al., 2014; Gomez et al., 2018, 2020; Lambeck et al., 2014; Lin et al., 2021;

105   Pittard et al., 2022; Simms et al., 2019; Whitehouse et al., 2012). To represent these uncertainties,

106   we use three different ice-sheet histories that span a plausible range of LGM ice-sheet thickness

107   reconstructions. The first ice history Golledge et al. (2014; henceforth Gol14) contains a deglacial

108   Antarctic Ice Sheet volume change of ~10.5 m global mean sea level equivalent (GMSLE), and

109   was run at 14 km resolution and 100 year timesteps-. Gol14 was created from the median of an

110   ensemble of Parallel Ice Sheet Model runs (Bueler and Brown, 2009) forced by an Earth system

111   model and uniform sea-level changes, and constrained by geologic observations such as ice-core

112   derived changes in regional ice thickness. The second ice history Whitehouse et al., (2012;

113   henceforth W12) contains a deglacial Antarctic Ice Sheet volume change of ~8 meters GMSLE

114   and was created by running the GLIMMER ice sheet model (Rutt et al., 2009) for discrete time

115   intervals (20, 15, 10, and 5 ka) with a 20 km resolution, and is constrained by glaciologic, geologic,

116   and Antarctic relative sea-level records. The third ice history Gomez et al. (2018; henceforth

117   Gom18) has a deglacial Antarctic Ice Sheet volume change of ~6 m GMSLE. The Gom18 model

118   is a single model run of a coupled, gravitationally consistent GIA-dynamic ice sheet model that

119   incorporates 3-D earth structure and was forced by climate via benthic $\delta^{18}O$ records. The ice sheet

120   model was run with 20 km resolution and 200 year timesteps.

121   These ice-sheet histories encompass a range of potential Antarctic Ice Sheet volume

122   changes (6–10.5 m GMSLE; Supplementary Figure S1) and therefore, a range of potential GIA

123   magnitudes across the Ross Sea Embayment. To simulate GIA for W12 and Gol14 we use a 1-D,

radially symmetric Earth model with a lithospheric thickness of 96 km, and an upper and lower mantle viscosity of 10^{21} Pa s and 10^{22} Pa s, respectively. Our Earth model is similar to the best fit 1-D Earth model used in Whitehouse et al. (2012), which was determined by inverting for the solid Earth rheology that best fit Antarctic deglacial sea-level data and is consistent with local constraints on upper mantle viscosity (Nield et al., 2016). We explore the sensitivity to our choice in Earth model by simulating GIA for W12 and Gol14 using two alternatives. One is the VM5a Earth model (lithosphere thickness of 96 km, average upper and lower mantle viscosity of 0.5 x 10^{21} and 1.6 x 10^{21}, respectively (Peltier et al., 2015). Additionally, we consider a lower-viscosity Earth model representative of West Antarctica, with a 50 km lithosphere and low viscosity zone of 10^{19} Pa·s from 50 km down to 200 km depth, viscosity of 0.2 x 10^{21} Pa s to 670 km depth, and lower mantle viscosity of 3 x 10^{21} Pa s (Pollard et al., 2017).

2.2 Simulating Grounding line Persistence

To determine the locations where grounding lines can persist in the Ross Sea Embayment, we first trace 147 LGM ice stream flowlines based on reconstructions of Anderson et al. (2014) and present-day ice-sheet flow (Rignot et al., 2011). From the ice divide to the present-day grounding line, ice flowlines are based on observed ice surface velocities (Rignot et al., 2011), and from the present-day grounding line to the edge of the continental shelf, ice flowlines ~~follows~~ follow paleo-ice flow reconstructions of ~~paleo-ice flow reconstructed of~~ Anderson et al., (2014). We consider the 20 ka bathymetry and present-day bathymetry to compare LGM and interglacial (i.e. present-day) endmembers. Although Ross Sea Embayment ice stream flowlines underwent localized reorganization throughout the last deglaciation (Greenwood et al., 2018; Lee et al., 2017), we use LGM flowlines when modeling grounding line persistence for both the 20 ka and present-day bathymetry to make clear comparisons between these time periods. By using LGM flowlines for both the 20 ka and present-day bathymetry, we can track zones of grounding line persistence throughout the entire Ross Sea. Although using LGM flowlines for present-day can result in predicting steady state stability at locations that are inconsistent with the observational record (e.g. predicting grounding line locations that do not correspond to the observed present day grounding line), ~~it~~this approach expands our understanding of solid Earth-ice sheet interactions in a way that would not be possible with traditional ice-sheet modeling methods.

We model the potential locations where grounding lines can persist for each ice stream flowline by first extracting its bathymetric profile for the present-day bathymetry and the 20 ka

155 bathymetries associated with each ice history. We then use a simple differential equation for the
156 mass balance of a marine-terminating ice stream (Equation 1 in Robel et al., 2018, following
157 Schoof 2012) to test for stability along each ice stream flowline at 500 m-spaced nodes. ~~We~~
158 ~~consider different combinations of accumulation, basal friction, and ice-shelf buttressing~~
159 ~~parameters (Table 1) by uniformly sampling the range of basal friction and ice-shelf buttressing~~
160 ~~and sampling the range of accumulation rates with a non-linear spacing, since they range over an~~
161 ~~order of magnitude; resulting in an ensemble of 2,000 linear stability analyses at each node along~~
162 ~~an ice stream flowline.~~
163
164 ~~The model is given by:~~

165 $$\frac{dL}{dt} = h_g(PL - \Omega h_g^\beta) \quad (1)$$

166

167 $$\frac{dL}{dt} = h_g(PL - \Omega h_g^\beta) \quad (1)$$

168
169 in which

170 $$\beta = \frac{m+n+3}{m+1} \quad (2)$$

171 $$\Omega = \frac{A(\rho_i g)^{n+1}\left(1 - \frac{\rho_i}{\rho_w}\right)^n}{(4^n C)^{\frac{1}{m+1}}} \Theta^{\frac{n}{m+1}} \quad (3)$$

$$\Omega = \frac{A(\rho_i g)^{n+1}\left(1 - \frac{\rho_i}{\rho_w}\right)^n}{(4^n C)^{\frac{1}{m+1}}} \Theta^{\frac{n}{m+1}} \quad (3)$$

172 $$h_g = -b\frac{\rho_w}{\rho_i} \quad (4)$$

173 Where P is the upstream averaged surface mass balance (0.01–0.3 m/yr; Buizert et al., 2015;
174 Cavitte et al., 2018), L is the distance of the node downstream from the ice divide, t is time, b is
175 bathymetric depth at the grounding line, h_g is ice thickness at the grounding line, and Ω is a scalar
176 that accounts for factors that affect grounding line flux such as C, the basal friction
177 (1.62–$6.62 Pa \cdot s^{-1}$), and Θ, ice-shelf buttressing (0.5–1.0; smaller values represent more
178 buttressing). A is the Nye-Glenn law coefficient ($2 \times 10^{-24} Pa \cdot s^{-1}$), n is the accompanying Nye-
179 Glen flow law exponent (3), m is the Weertman friction law exponent ($\frac{1}{3}$), ρ_i is the density of ice

180 (917 $\frac{kg}{m^3}$), ρ_w is the density of sea water (1028 $\frac{kg}{m^3}$), and g is gravitational acceleration (9.81 $\frac{m}{s^2}$).

181 We consider different combinations of accumulation, basal friction, and ice-shelf buttressing

182 parameters (Table 1) by uniformly sampling the range of basal friction and ice-shelf buttressing

183 and sampling the range of accumulation rates with a non-linear spacing, since they range over an

184 order of magnitude; resulting in an ensemble of 2,000 linear stability analyses at each node along

185 an ice stream flowline.

186 We allow for ice-shelf buttressing given evidence for the formation of ice shelf

187 embayments in both the East and West Ross Sea (e.g. Bart et al., 2018; Prothro et al., 2020), and

188 our average upstream surface mass balance values are consistent with local ice core and ice

189 penetrating radar records (Buizert et al., 2015; Cavitte et al., 2018). The form of the grounding line

190 flux (Ωh_g^β) is taken from prior asymptotic approximation studies of ice flux at grounding lines

191 (e.g., Schoof, 2007; Haseloff and Sergienko, 2018), and is appropriate to use here since we only

192 analyze the steady-state of Equation 1. The form used here assumes a given Weertman-style basal

193 friction law, no lateral shear stress, and buttressing from an ice shelf of fixed size. While other

194 forms of the grounding line flux (Haseloff and Sergienko, 2018) may be used, the results here are

195 unlikely to be strongly dependent on the particular form used as long as there is a strong

196 dependence on bathymetry (as occurs in existing grounding line flux approximations, e.g. Schoof

197 2007).

198 A node is a potential "stable steady-state" if two conditions are met: (1) the ice flux into

199 the node is equal to ice flux out ($\frac{dL}{dt} = 0$ in Equation 1), and (2) the first derivative of the right-

200 hand side of Equation 1 with respect to L is negative (i.e. perturbations to the grounding line

201 position return the grounding line to its original position). This is expressed as:

202
$$Ph_g^{-1} + \left[PLh_g^{-2} + (\beta - 1)\Omega h_g^{\beta-2}\right]\frac{\rho_w}{\rho_i}\frac{dh}{dL} < 0 \tag{5}$$

203 These conditions constitute a linear stability analysis of the grounding line position (Schoof

204 2012; Robel et al. 2018).

205

Table 1: Parameters used in Equations 1-5		
Parameter	Description	Value
L	Distance downstream from ice divide (m)	-
h_g	ice thickness at the grounding line (m)	-
b	Topographic elevation at the grounding line (m)	-
P	upstream average surface mass balance $(\frac{m}{yr})$	0.01-0.3
A	Nye-Glen law coefficient $(Pa^{-n} \cdot s^{-1})$	$2 \cdot 10^{-24}$
m	Weertman friction law exponent	$\frac{1}{3}$
n	Nye-Glen law exponent	3
C	Basal friction coefficient $(Pa \cdot m^{\frac{-1}{n}} \cdot s^{\frac{1}{n}})$	1.62 - 6.62·10^6
Θ	Ice shelf Buttressing parameter	0.5-1
ρ_i	Ice density $(\frac{kg}{m^3})$	917
ρ_w	Sea water density $(\frac{kg}{m^3})$	1028
g	Gravitational acceleration $(\frac{m}{s^2})$	9.81

206

Table 1: Parameters used in Equations 1-5		
Parameter	Description	Value
L	Distance downstream from ice divide (m)	-
h_g	ice thickness at the grounding line (m)	-
b	Topographic elevation at the grounding line (m)	-
P	upstream average surface mass balance ($\frac{m}{yr}$)	0.01-0.3 (n=20)
A	Nye-Glen law coefficient ($Pa^{-n} \cdot s^{-1}$)	$2 \cdot 10^{-24}$
m	Weertman friction law exponent	$\frac{1}{3}$
n	Nye-Glen law exponent	3
C	Basal friction coefficient ($Pa \cdot m^{\frac{-1}{n}} \cdot s^{\frac{1}{n}}$)	1.62 - 6.62·10^6 (n=10)
Θ	Ice shelf Buttressing parameter	0.5-1 (n = 10)
ρ_i	Ice density ($\frac{kg}{m^3}$)	917
ρ_w	Sea water density ($\frac{kg}{m^3}$)	1028
g	Gravitational acceleration ($\frac{m}{s^2}$)	9.81

Table 1 | Parameters and values used for linear stability analysis.

As prior studies have argued (Robel et al., 2022; Sergienko and Haseloff, 2023), the dynamic nature of climate, ice sheets, and the solid Earth make it unlikely that grounding lines will achieve a mathematically stable steady-~~states~~state in the real world. However, linear stability analysis provides a useful guide to identify locations where grounding lines were likely to have persisted or slowed ~~down~~ retreat for prolonged ~~time~~ periods without information about where the ice margin existed geologically at any time, since information about the age and location of past grounding lines is uncertain.

Along each ice stream flowline bathymetry, our ensemble analysis predicts "stable steady-state" grounding line locations for different combinations of surface mass balance, ice shelf buttressing, and basal friction coefficient (P,θ, C; Table 1). Thus, our predicted "stable steady-state" locations are not the grounding line location at any given time, but rather where—for a combination of P, θ and C—an ice stream grounding line could achieve mathematical stability. We

221   interpret the parts of each flowline that contain more "stable steady-state" grounding line locations

222   as being zones where the grounding line can persist across a wider range of glacial and climate

223   conditions (zones of potential persistence; ZPP), either at present-day or 20 ka, for an extended

224   period of time. Once we predict steady stable state grounding lines along a bathymetric transect,

225   we explore the impact of grid resolution by resampling the bathymetric transect at progressively

226   coarser grid resolutions and repeating the linear stability analysis. We resample by smoothing the

227   transect using a windowed mean of the desired resolution and then resampling the smoothed

228   bathymetry at the desired resolution.

229   To validate the results from our simple model of grounding line persistence, we also

230   modeled transient grounding line evolution with a 1-D flowline model of marine ice-sheet

231   evolution, using the shallow-shelf approximation (Robel, 2021; Schoof, 2007). This model

232   provides an alternative method to identifying the role of GIA for transient cases that do not attain

233   a strict steady-state, and which do not require most of the assumptions intrinsic to Equation 5 (e.g.

234   grounding line dynamics are a smooth system). We calculate grounding line retreat rates and

235   grounding line discharge over the 20 ka and present-day bathymetries and compare spatial patterns

236   of transient grounding line retreat and discharge between the 20 ka and present-day bathymetries

237   (Supplementary Material). Our transient modeling mirrors our results with the stability analysis;

238   we find that grounding line discharge decreases, and grounding line retreat rates slow at the same

239   locations where we predict zones of potential persistence with our simpler model (Supplementary

240   Material; Figure S2). These similarities are not surprising since the model captured by Equations

241   1-3 is designed to approximate more complex ice sheet models at steady states.

242

243   **3.   Results and discussion**

244   **3.1 Patterns of GIA across the Ross Sea Embayment**

245   From 20 ka to present-day, all three ice histories result in a relative sea-level (RSL) fall due

246   to GIA uplift of the Ross Sea Embayment interior (Figure 1a–c). The ice histories with larger

247   excess LGM ice volume cause a larger RSL change, with a maximum RSL change of -140 m and

248   -170 m (Figure 1a; Figure 1b), for W12 (GMSLE = 8 m) and Gol14 (GMSLE = 10.5 m; Figure

249   S3), respectively. The interior of the Ross Sea Embayment, offshore of the Siple Coast (SC, Figure

250   1e) experiences the maximum uplift in both of these ice histories. In contrast, Gom18 produces a

251   smaller magnitude of uplift in the Ross Sea Embayment (RSL fall of -115 m; Figure 1c), with two

centers of maximum uplift: one offshore of the Siple Coast (Figure 1c) and the other near Northern

Victoria Land (NVL; Figure 1c). The different pattern of GIA-induced uplift results from the lower

viscosity in the Ross Sea Embayment used in Gom18 compared to the higher-viscosity 1-D Earth

structure used in simulations of W12 and Gol14, in addition to differences in the ice loading history

(Figure 1a–c; Figure S4; Gomez et al., 2018).
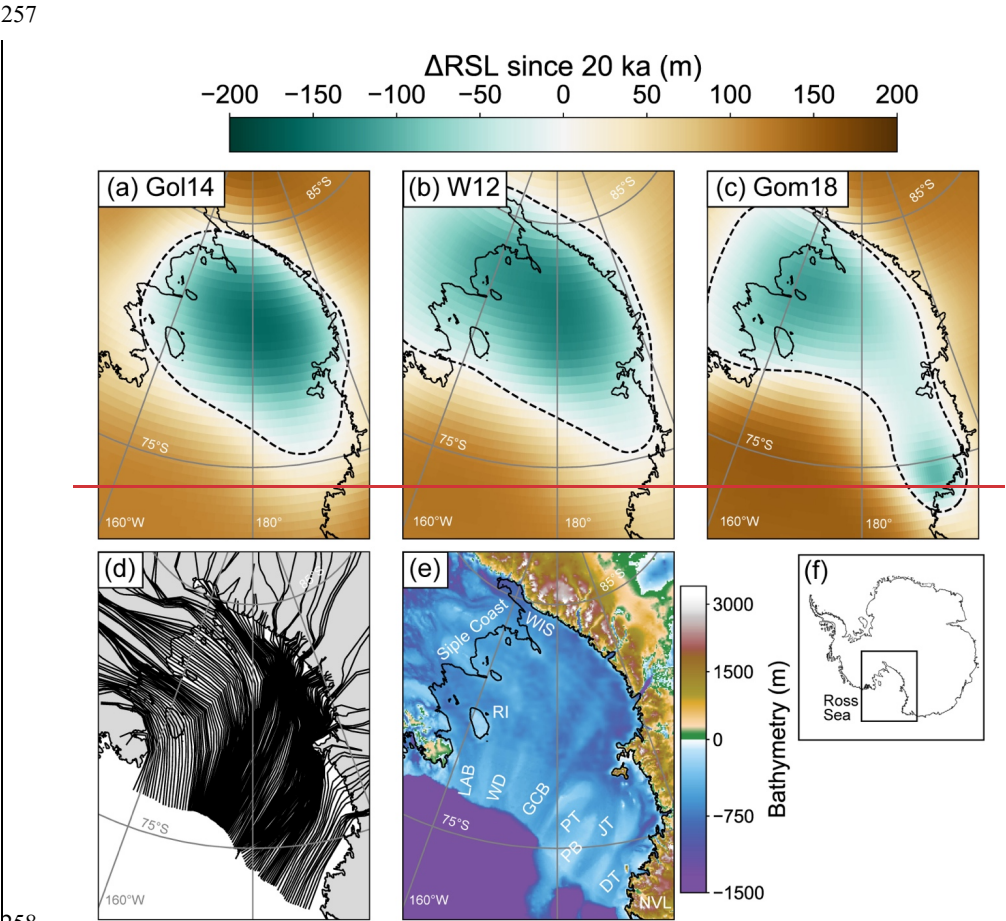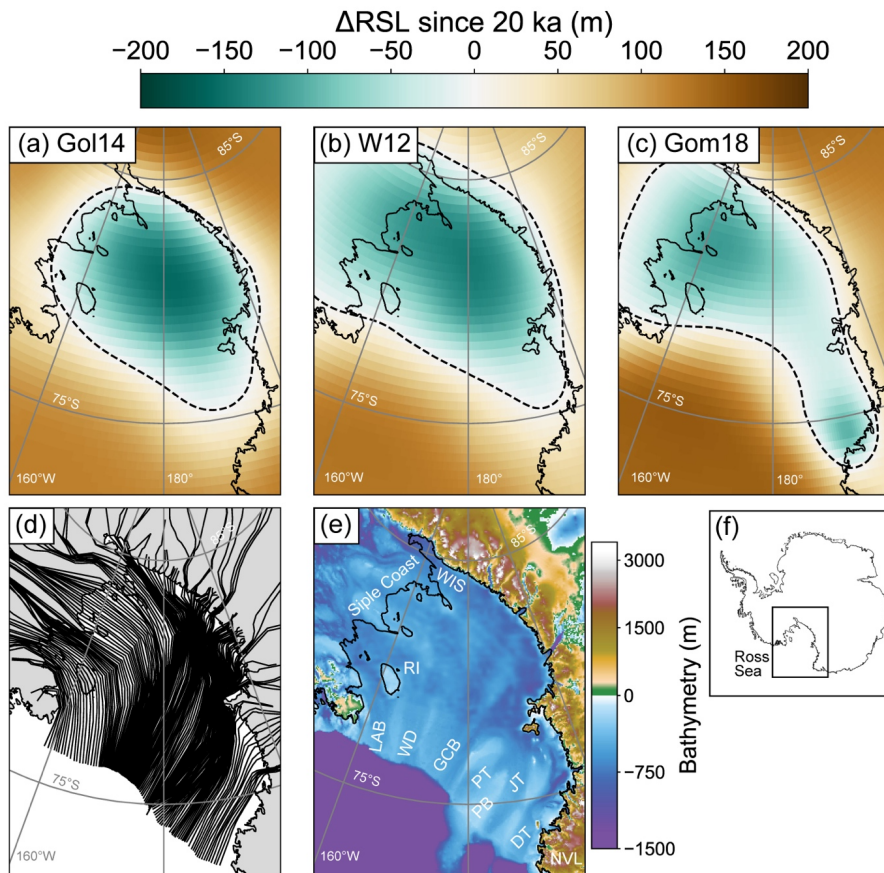
Figure 1 | Change in relative sea level (𝟛RSL) from 20 ka to present-day for a) Gol14 b) W12 and c) Gom18. Solid black line is the present-day grounding line and dashed black line marks the zero-contour line of 𝟛RSL since 20 ka. d) Last Glacial Maximum ice stream flowlines based on Anderson et al. (2014) and Rignot et al. (2011). e) Present-day bathymetry of the Ross Sea Embayment (Morlighem et al., 2020). LAB – Little America Basin, WD – Wales Deep, GCB – Glomar Challenger Basin, PT – Pennell Trough, PB – Pennell Bank JT – JOIDES Trough, DT – Drygalski Trough, RI – Roosevelt Island, NVL – Northern Victoria Land, WIS – Whillans Ice Stream. f) Inset of Antarctica. Black box shows extent of panels a-e. Solid black line represents present-day grounding line from MEaSUREs (Rignot et al., 2011)

3.2 The impact of GIA on Grounding Line Persistence from 20 ka to present-day

272   Next, we quantify how GIA impacts where grounding lines can persist. For each ice stream,

273   our ensemble analysis predicts the locations of "stable steady~~-~~state" grounding line positions for

274   a given bathymetry (20 ka and present-day) and set of parameter values. For example, Figure 2b

275   shows the count of potential stable steady-state grounding lines associated with the reconstructed

276   bathymetric transect for the paleo-Whillans ice stream (Fig. 2a) corrected for GIA (Gom18–

277   orange, W12–purple, Gol14–red; Figure 2b), compared to the present-day bathymetry (black;

278   Figure 2b). Present-day bathymetry contains a higher count of potential stable steady states

279   upstream of the flowline, close to the present-day grounding line (black; ~~figure~~Figure 2B),

280   compared to any of the 20 ka bathymetries corrected for GIA (orange, purple, and red; Figure 2b),

281   which contain higher counts of potential stable steady states near the edge of the continental shelf.

282   Zones along the transect with higher counts of potential stable grounding line locations are

283   stable across a wider range of input parameter combinations and therefore have a relatively higher

284   likelihood of persisting at that location regardless of parameter uncertainty and are referred to as

285   "zones of potential persistence (ZPP). Each zone contains the count of potential stable grounding

286   lines within a 50 km reach along a given ice stream flowline (Figure 2b). The present-day

287   bathymetry has zones of potential persistence near the present-day grounding line (~750 km

288   downstream; black; Figure 2b), whereas each 20-ka bathymetry has zones of potential persistence

289   near the continental shelf break (~1600 km downstream; orange, purple, and red; Figure 2b).

290   To quantify how zones of potential persistence shift across the deglaciation, we calculate

291   the percent change in the number of stable steady-state stable grounding lines within a given 50-

292   km reach of an ice stream transect from 20 ka to present-day. We calculate the percent change of

293   zones of potential persistence along eight flowlines divided into 50 km reaches, and find that,

294   similar to predictions for the paleo-Whillans ice stream, zones of potential persistence decrease

295   near the continental shelf break and increases further upstream from 20 ka to present-day (Figure

296   2c-e).

297
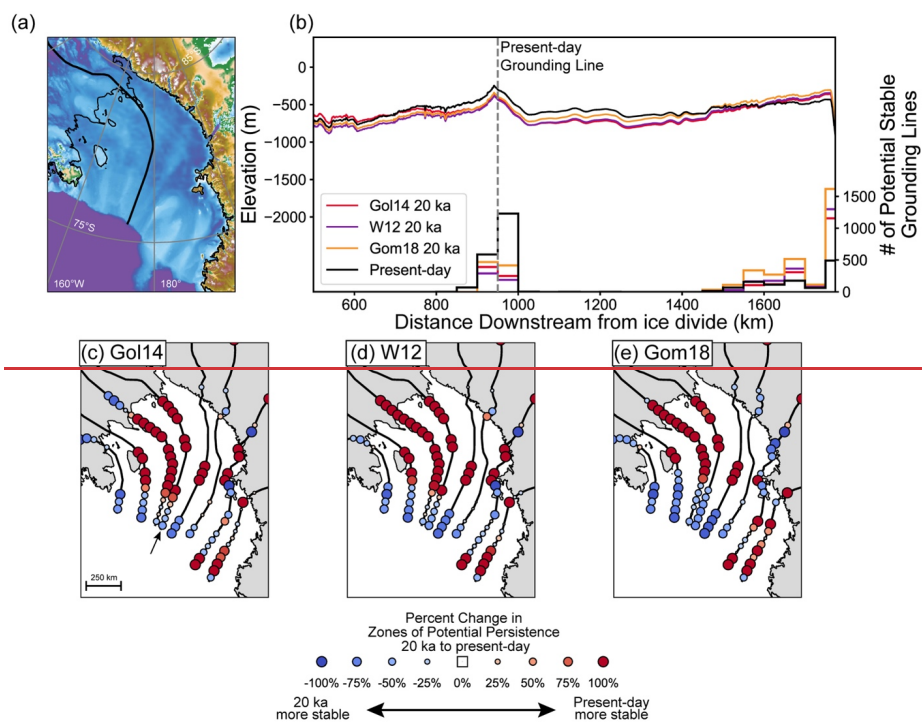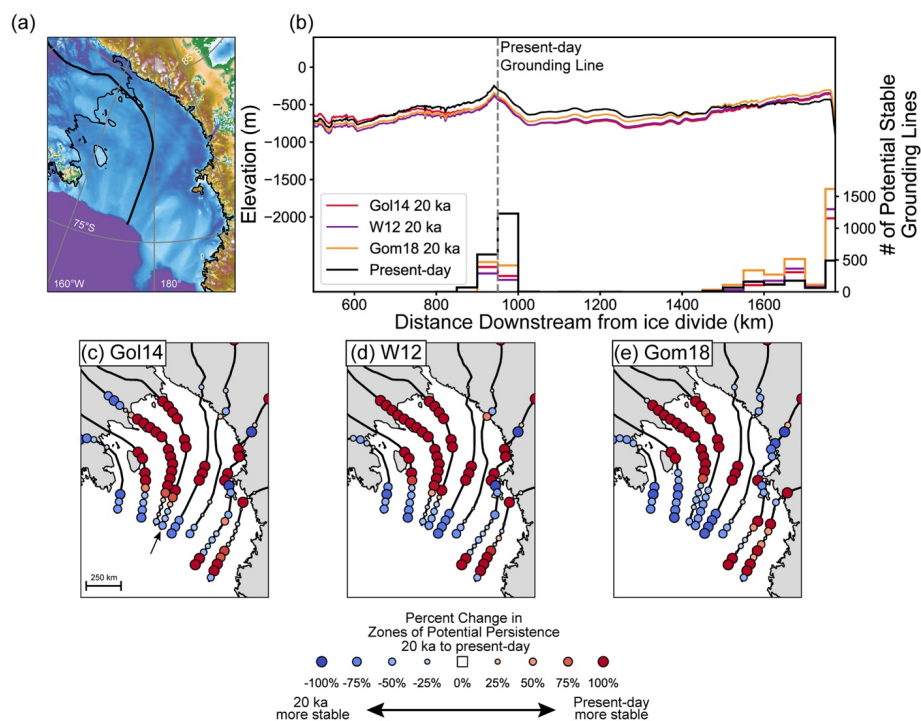
Figure 2 | Zones of potential persistence (ZPP) along individual flowlines. a) Flowline path of the paleo-Whillans ice stream and present-day bathymetry of the Ross Sea Embayment (Morlighem et al., 2020). b) Present-day bathymetry (black), and 20 ka GIA-corrected paleobathymetry for W12 (purple), Gol14 (red), and Gom18 (orange) along the paleo-Whillans ice stream flowline with corresponding histograms of simulated stable grounding line positions. Histograms and corresponding bathymetry share color. c-e) Percent change in the number of modeled potential stable grounding line from 20 ka (LGM) bathymetry to present-day bathymetry for Gol14 (c), W12 (d), and Gom18 (e) ice histories. Arrow in panel c denotes flowline used in panel b.

We then expand our grounding line stability analysis to all 147 ice stream flowlines. We bin stable steady-state grounding ~~line zones into~~lines within a 20 km x 20 km grid to identify zones of potential persistence for the 20 ka and present-day bathymetries and calculate the percent change of zones of potential persistence from 20 ka to present-day (Figure 3). From 20 ka to present-day, there are fewer zones of potential persistence near the edge of the continental shelf (these locations were more stable during the LGM; blue; Figure 3), and more zones of potential

persistence upstream, suggesting these locations are more stable during present-day (red and purple; Figure 3). The general pattern of downstream decrease in zones of potential persistence across the deglaciation is interspersed with isolated regions of increased or minimal change in zones of potential persistence, corresponding to ridges separating the Little America Basin, Wales Deep, and Glomar Challenger Basin (LAB, WD, GCB; Figure 4c; Figure 1e). The Gom18 model predicts slightly different patterns compared to the Gol14 and W12 models, with the decrease in zones of potential persistence extending further upstream and a larger area of increased zones of potential persistence near the JOIDES and Drygalski troughs (JT, DT; Figure 1e) caused by the second center of maximum uplift.

There are two GIA mechanisms that cause the locations of zones of potential persistence to shift upstream over the last deglaciation: 1) sea-level fall caused by rebound of the solid Earth under the locus of ice mass loss (~250 m) and 2) sea-level rise caused by global ice sheet melt (~130 m), and secondarily by the collapse of the Antarctica peripheral bulge (~10 m; Figure S3). Within the interior of the Ross Sea Embayment, relative sea-level fall caused by isostatic rebound is nearly twice the magnitude of sea-level rise caused by global ice sheet melt. In contrast, near the continental shelf edge, relative sea-level rise is dominated by global ice sheet melt while peripheral bulge collapse contributes <10% of the signal.

Isostatic rebound shoals bathymetry within the interior of the Ross Sea Embayment shoals bathymetry, decreasing flux through the grounding line, thus increasing the potential for a "stable steady-state" grounding line. Near the continental shelf edge changes relative sea-level rise is predominately caused by global ice sheet melt and peripheral bulge collapse contributes <10% of the signal. at present-day. Sea-level rise caused by far field ice sheet melt and Antarctic peripheral bulge collapse causes increased grounding line flux, which decreases the likelihood of a "stable steady state" grounding line position near the edge of the continental shelf at present day (Figure 3).

Together, these GIA mechanisms cause a net upstream migration of zones of potential persistence. During the LGM the grounding line was located near the edge of the continental shelf, and at present-day the grounding line is located within the Ross Sea Embayment interior. Our analysis shows that GIA promotes grounding line stability near the edge of the continental shelf during the LGM and promotes grounding line stability within the Ross Sea Embayment interior at present-day. The co-occurrence of inferred locations of the grounding line for present-day and

346 ~~LGM suggests GIA stabilizes the grounding line at both glacial maximum and interglacial climate~~
347 ~~states~~

348   At present-_day, GIA has caused the interior of the Ross Sea Embayment to rebound,
349 resulting in the emergence of zones of potential grounding line persistence co-located with the
350 present-day grounding line. These zones of potential persistence located near the present-day
351 grounding line are less prevalent at 20 ka due to isostatic depression and predominately do not
352 emerge until the mid-Holocene (~5 ka; Supplementary Figure S5) for all ice histories, suggesting
353 that large magnitudes of isostatic rebound over a prolonged period (i.e., deglacial timescale)
354 provides persistence at the present-day grounding line location.

355   Our analysis shows that GIA promotes grounding line stability near the edge of the
356 continental shelf during the LGM and promotes grounding line stability within the Ross Sea
357 Embayment interior at present-day. ~~Similarly, global~~The co-occurrence of inferred locations of the
358 grounding line for present-day and LGM suggests GIA stabilizes the grounding line at both glacial
359 maximum and interglacial climate states

360   Global-scale ice ~~sheet changes support~~sheets reinforce zones of potential persistence at the
361 LGM grounding line. ~~Near complete loss~~The occurrence of zones of potential persistence ~~from~~at
362 20 ka ~~to present-day~~ within the deep submarine troughs of the Ross Sea Embayment (~~red;~~ Figure
363 3) is due to lower LGM relative sea level caused by Northern Hemisphere ice-sheet growth (and
364 the resulting global sea-level lowstand). Simulations that ignore Northern Hemisphere ice sheets
365 underestimate zones of potential persistence at 20 ka by up to 100% (Supplementary Figure S4),
366 emphasizing the importance of large Northern Hemisphere ice sheets for stabilizing the LGM
367 grounding line at the continental shelf edge.~~ By increasing grounding line stability towards the~~
368 ~~continental shelf edge, lower LGM relative sea level due to large ice sheet volumes in the Northern~~
369 ~~Hemisphere may be responsible for~~ and potentially driving larger LGM ice volume in the Ross
370 Sea Embayment.

371   Our finding, that zones of potential persistence increase at the Ross Sea Embayment LGM
372 grounding line due to GIA, parallels the finding that far-field ice-sheet retreat has an important
373 feedback on Antarctic Ice Sheet deglaciation (Gomez et al., 2020). While previous studies focused
374 on the influence of GIA on transient grounding line retreat (solid Earth feedbacks due to ice mass
375 loss at a given time step; de Boer et al., 2014; van Calcar et al., 2023; Gomez et al., 2013, 2015,

376 2018; Konrad et al., 2015; Pollard et al., 2017), our analysis instead provides a window into how

377 GIA reinforces the grounding line at endmember glacial-interglacial time frames.

378
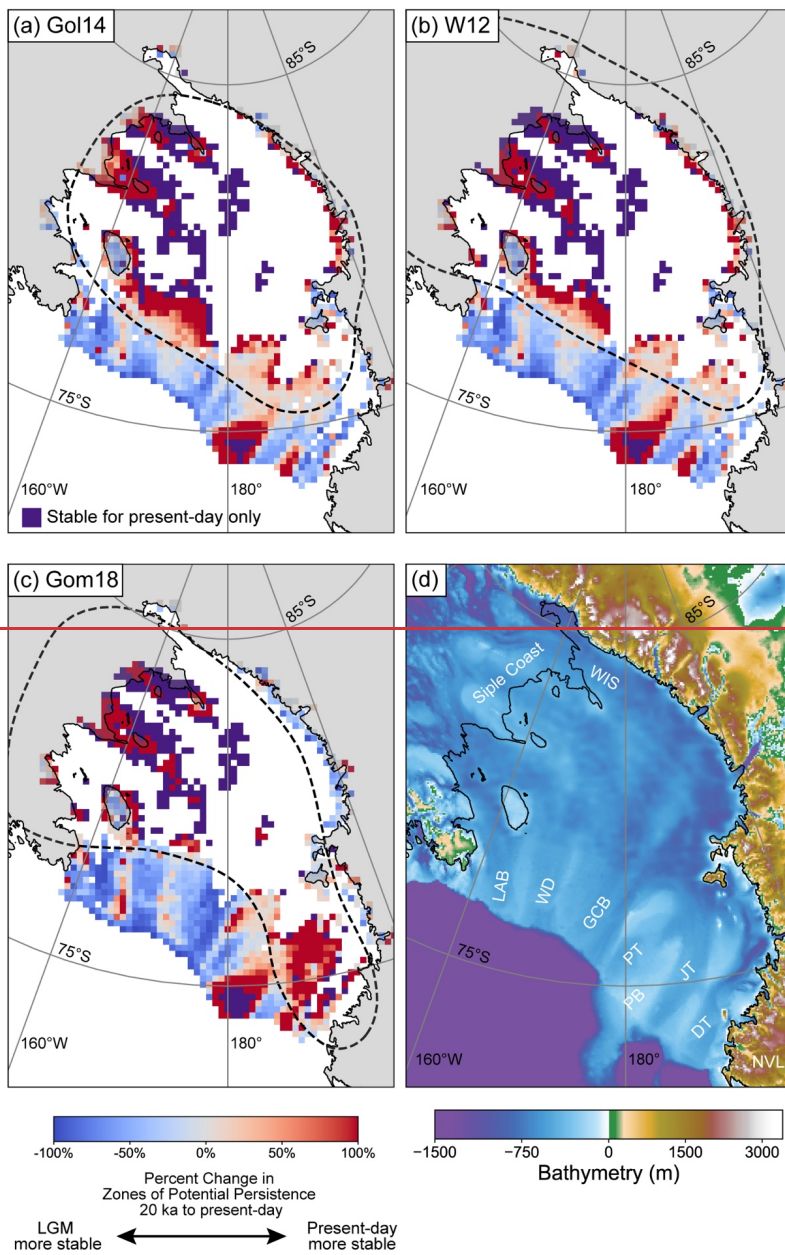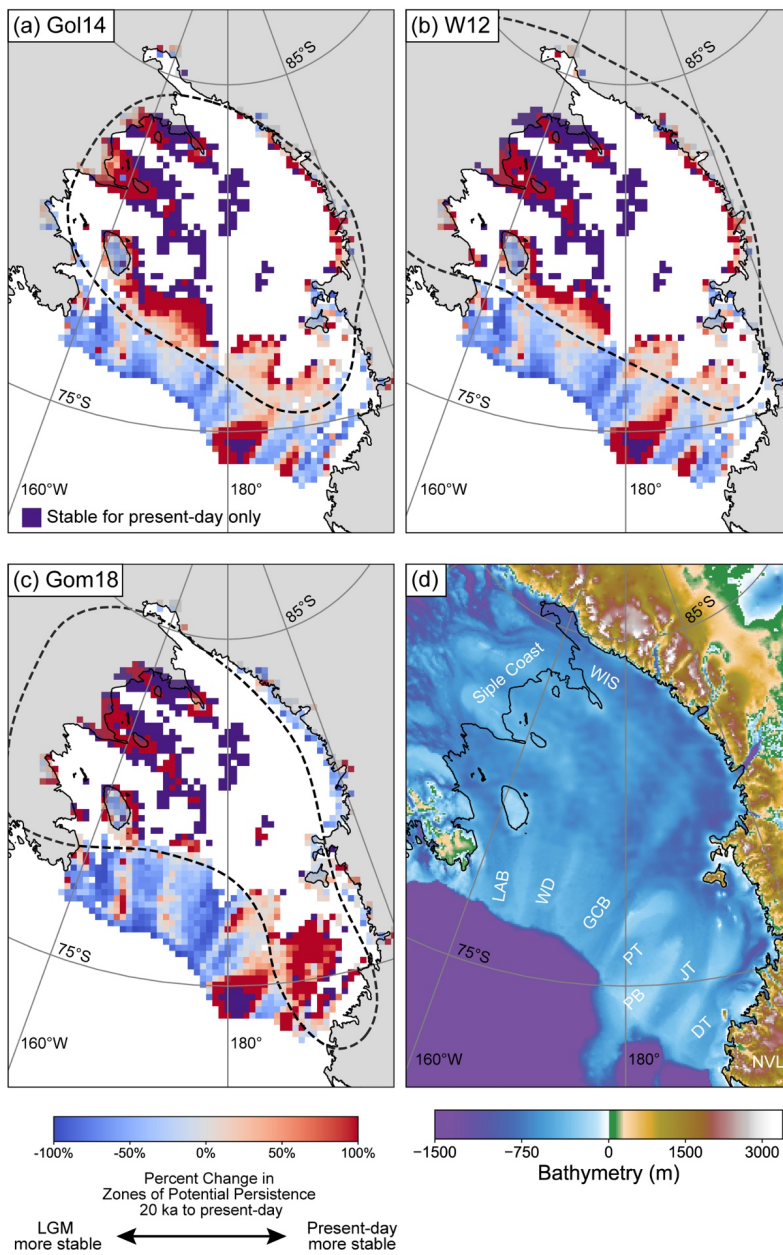
Figure 3 | GIA-induced percent change in ~~stable grounding line positions~~zones of potential persistence (ZPP) across 20 km x 20 km grid cells for entire Ross Sea Embayment based on glacial isostatic adjustment simulations for a) Gol14, b) W12, and c) Gom18. Grid cells that have stable steady-state grounding line positions in the present-day and no stable steady-state stable grounding line positions at 20 ka are marked in ~~teal~~purple. Thin black line is present-day day grounding line and dashed line is ~~transition from sea-level fall (within) to sea-level rise (outside).~~the zero-contour line of ΔRSL since 20 ka. d) Present-day bathymetry of the Ross Sea Embayment (Morlighem et al., 2020).

3.3 Characteristic Stable Grounding Line depth for the Ross Sea Embayment

GIA moves zones of potential persistence by modulating the bathymetry of the Ross Sea Embayment. However, bathymetry is only one of the parameters that determines where grounding line persistence occurs. Grounding line persistence is a function of surface mass balance (P), ice shelf buttressing (θ), basal friction (C), distance downstream from the ice divide (L), and ice thickness at the grounding line (h_g). Therefore, for a given combination of input parameters (Table 1), there is an ice thickness h_g (and equivalent grounding line depth b) that produces a stable grounding line position (Figure 4a and Figure S5). Our linear stability analysis shows that stable grounding line depth is a function of the other input parameters (Figure 4a; Supplementary Figure S6). For instance, distance downstream from the ice divide and average upstream surface mass balance rate are both negatively correlated with grounding line depth (Figure 4a). Therefore, the depths at which we predict stable grounding lines are a function of both the deglacial climate system, and the geometry of the Antarctic Ice Sheet. As a result, the mean stable grounding line depths for the 20 ka bathymetry and present-day bathymetry are similar (Figure 4a). These mean depths are significantly different from the bathymetry we input into the simple model of grounding line persistence (Figure 4, grey; t-test; $p_{present-day}$, p_{W12}, p_{Gol14}, $p_{Gom18} < 0.001$), showing that the depth range at which our simple model finds persistence depends on our input parameters and the ice flowline geometry of the Ross Sea Embayment. Therefore, we infer that zones of potential persistence migrate spatially due to GIA by causing bathymetry to be uplifted or subsided into and out of this characteristic depth range (Figure 4c).

411
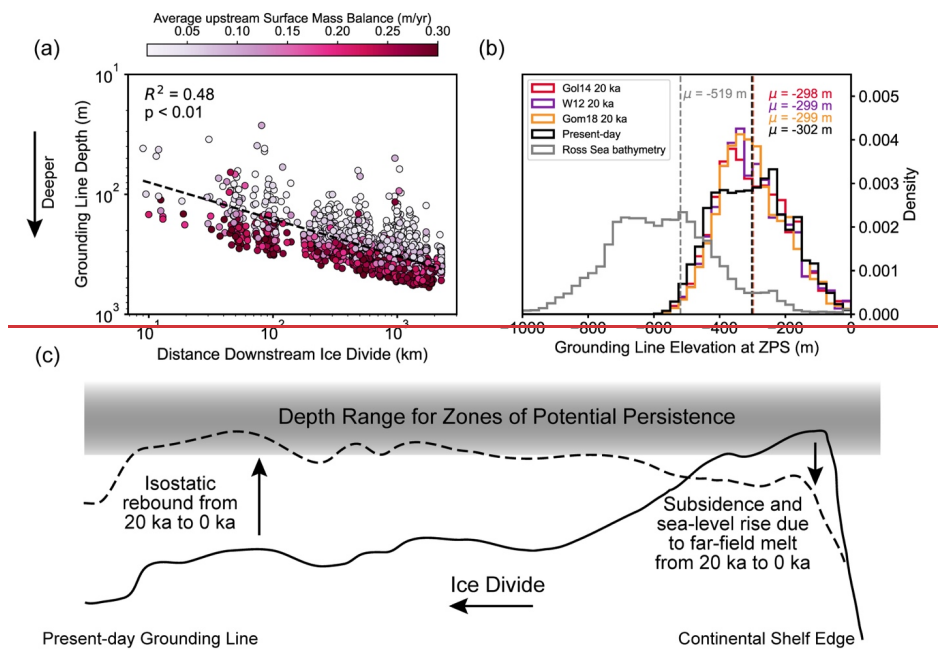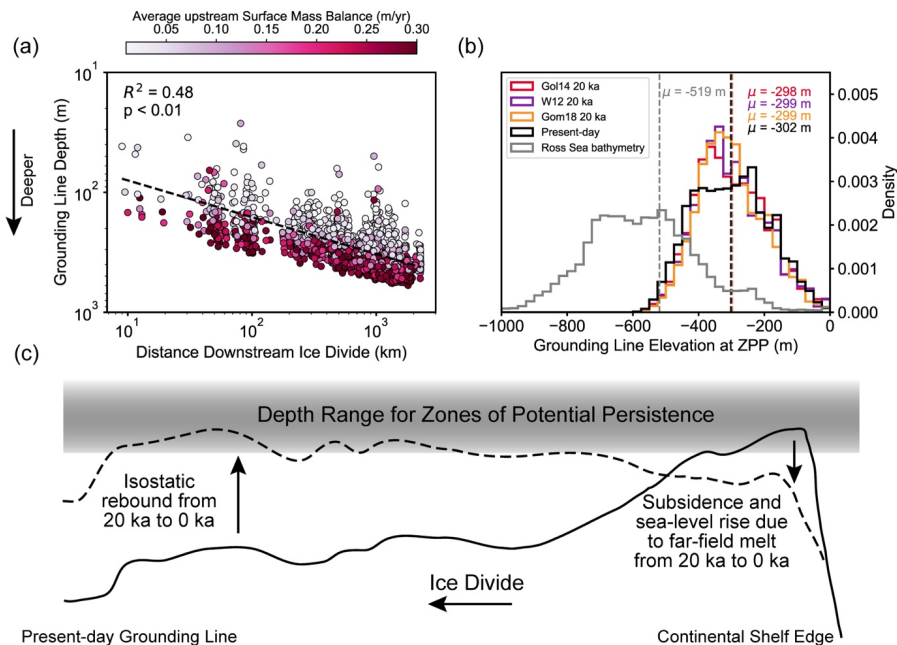
Figure 4 | a) Average upstream surface mass balance at distance downstream of the ice divide and grounding line elevation for ~~steady-state~~ stable grounding line positions on present-day bathymetry. **b)** Histograms of elevations for the ~~Present~~present-day bathymetry of the Ross Sea Embayment (grey), ~~steady-state~~ stable grounding line ~~positions~~elevation simulated ~~over~~for present-day bathymetry (black), and 20 ka paleobathymetry corrected for glacial isostatic adjustment based on the ice histories of Gol14 (red), Gom18 (orange), and W12 (purple). **c)** Schematic illustrating how glacial isostatic adjustment moves bathymetry into and out of ~~depth range for zones of~~ potential ~~stable grounding line elevations~~persistence.

3.4 Influence of grid resolution on predicted zones of potential persistence

To explore the effects of grid resolution, we use high resolution (500 m; Morlighem et al., 2020) bathymetry and resample to coarser resolution (up to 40 km~~; see Section 2.2), comparing~~), to compare how predicted zones of potential persistence vary across the Ross Sea (Fig. 5). Some of the datasets constraining bathymetry in the Ross Sea Embayment are gravity-based and therefore have a true resolution coarser than the 500 m output resolution of BedMachine. Nonetheless, we decide to treat BedMachine as 500 m resolution in the Ross Sea Embayment to explore the potential impacts of grid resolution. We predict fewer zones of potential persistence across the Ross Sea Embayment at 20 ka and present-day when using the coarse grid resolution

431 (20 km; Fig. 5b/c). Predictions with coarse resolution bathymetry largely fail to produce zones of

432 potential persistence near the edge of the continental shelf (Fig. 5c). Furthermore, the coarse

433 resolution prediction fails to predict zones of potential persistence near the present-day grounding

434 line on the present-day bathymetry (Fig. 5f).

435
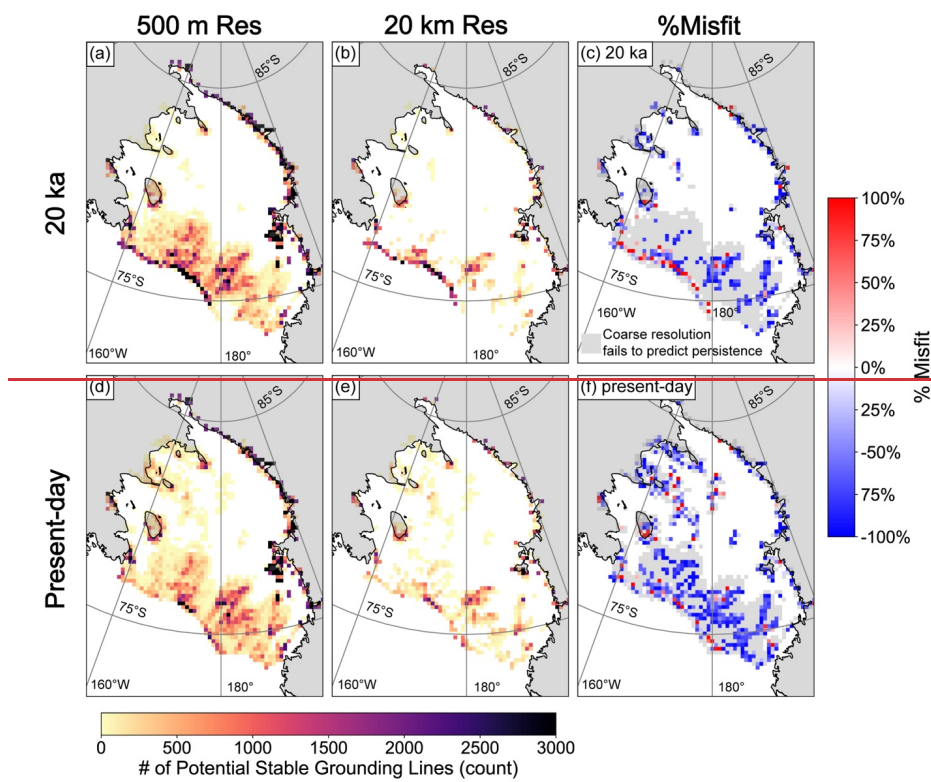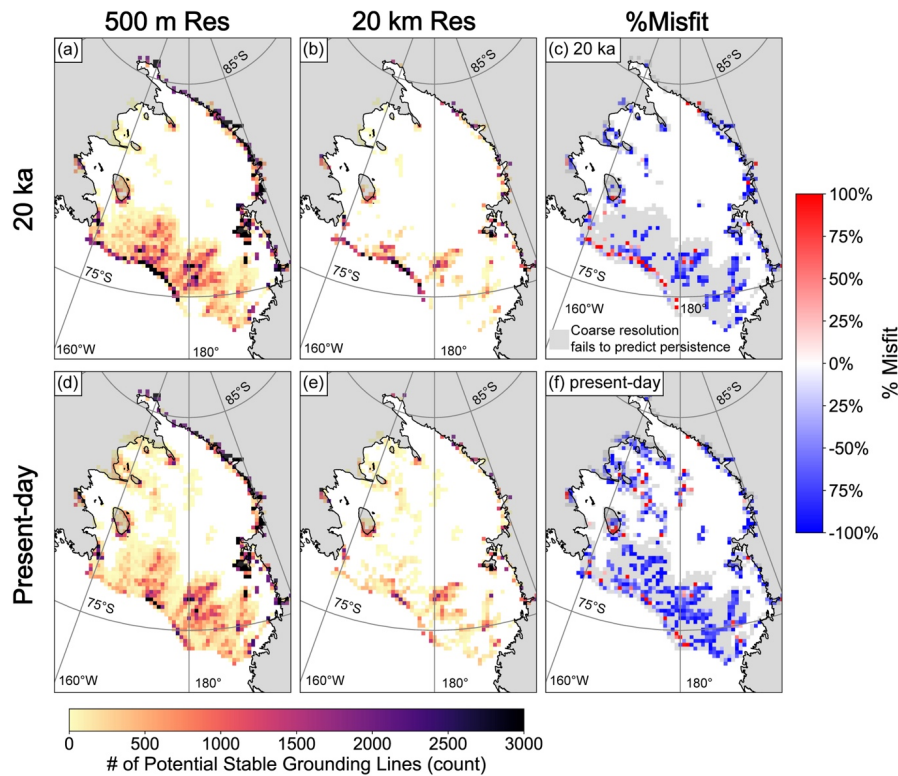
Figure 5 | ~~Density~~Zones **of** ~~stable grounding line positions~~potential persistence **for Gom18 Last Glacial Maximum (20 ka) (top row), Present-day (bottom row) for high resolution (50m; a/d) and low resolution (20 km; b/e) Percent misfit for 20 ka (c) and present-day (f), defined as difference of zones of potential persistence calculated using high resolution and coarse resolution bathymetry divided by zones of potential persistence calculated using high resolution bathymetry** $\left(\frac{ZPP_{500m} - ZPP_{20km}}{ZPP_{500m}}\right)$**. Light grey shows where coarse resolution fails to predict persistence.**

Since coarse grid resolution underpredicts zones of potential persistence for 20 ka and present-day bathymetry, coarse grid resolution will also underpredict how GIA migrates zones of potential persistence across the deglaciation. We quantify how coarse grid resolution underpredicts the impact of GIA by calculating the change in zones of potential persistence from 20 ka to present-day (Fig. 3), but with coarser grid bathymetric resolution (20 km). Figure 6a shows the percent

450 misfit for change in zones of potential persistence from 20 ka to present day of 20 km resolution

451 compared to 500 m resolution~~, with percent misfit defined as the fractional change of zones of~~

452 ~~potential persistence calculated using high resolution and coarse resolution bathymetry~~

453 ~~$\frac{ZPP_{500m}-ZPP_{20km}}{ZPP_{500m}}$~~ . $(\frac{\Delta ZPP_{500m}-\Delta ZPP_{20km}}{\Delta ZPP_{500m}})$.

454   We find that the coarse resolution bathymetry underpredicts the impact of GIA near the

455 present-day grounding line (blue; Fig 6a) and fails to capture the impact of GIA within most of the

456 deep submarine troughs (grey; Fig 6a), suggesting that high resolution bathymetry may be

457 necessary to fully quantify the role of GIA in potential retreat and readvance scenarios in the Ross

458 Sea Embayment (Balco et al., 2023; Kingslake et al., 2018; Lowry et al., 2024; Neuhaus et al.,

459 2021; Nichols et al., 2024; Venturelli et al., 2020). We also vary the coarseness of the grid

460 resolution and find that, as grid resolution coarsens, percent misfit converges towards ~80-90%

461 (compared to 500 m bed resolution; Figure 6b), highlighting the need for fine grid resolution to

462 capture interactions between GIA and bathymetry. The importance of bed resolution is, in part,

463 due to the broad scale retrograde slope of the Ross Sea Embayment bathymetry. In our linear

464 stability analysis, local prograde slope is one of the two conditions needed to achieve linear

465 stability (Equation 5). A coarse grid resolution smooths over small-scale (≤5 km) bathymetric

466 pinning points, which provide local prograde slope, in addition to smoothing over regions of

467 locally shallower grounding line depth. Based on our analysis, compared to 500 m grid resolution,

468 a grid resolution of 20 km leads to a ~95% misfit, while a grid resolution of 1 km leads to a ~25%

469 misfit (Fig. 6b).
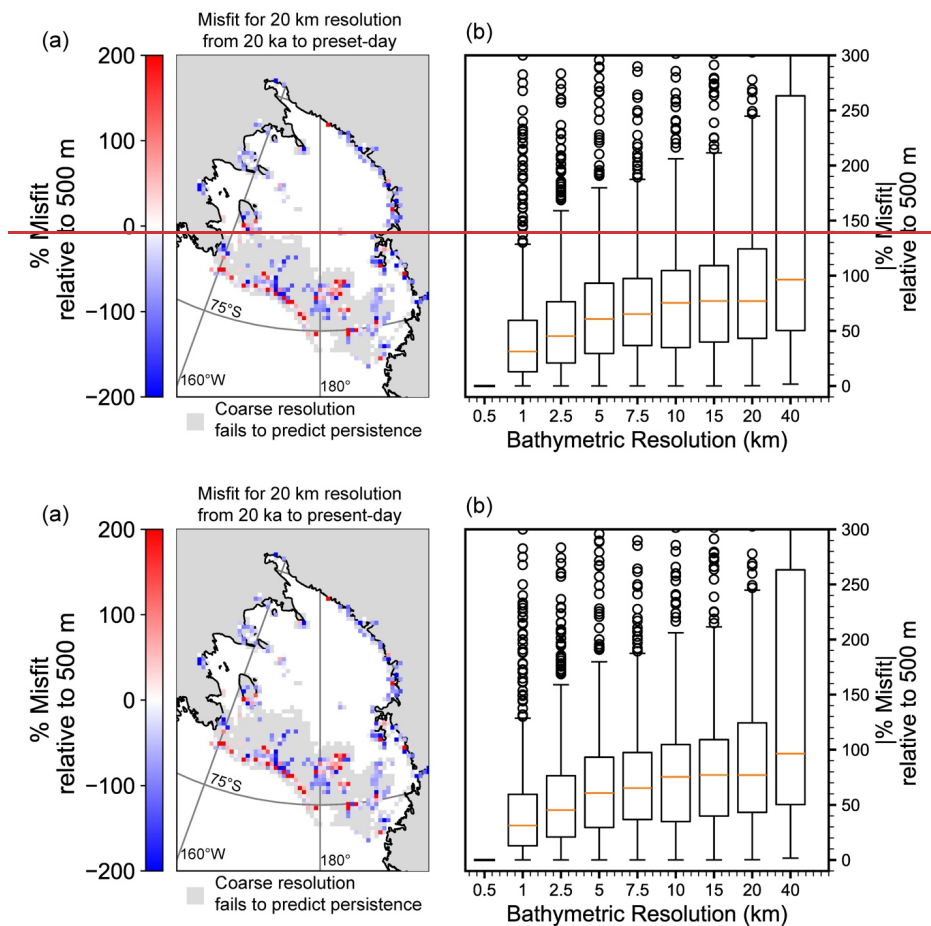
Figure 6 | a) Misfit of 20 km resolution compared to 500 m resolution for ~~grounding line~~predicted zones of potential persistence from 20 ka to present-day. Percent misfit defined as difference of ~~stable grounding line positions~~zones of potential persistence calculated using high resolution and coarse resolution bathymetry divided by ~~stable grounding line positions~~zones of potential persistence calculated using high resolution bathymetry

$$\left(\frac{ZPS_{500m} - ZPS_{20km}}{ZPS_{500m}}\right) \cdot \left(\frac{\Delta ZPP_{500m} - \Delta ZPP_{20km}}{\Delta ZPS_{500m}}\right).$$

Light grey shows where coarse resolution fails to predict stability. b) Magnitude distribution of percent misfit between zones of potential persistence calculated with 500 m resolution bathymetry and coarser bathymetry resolutions.

3.5 Comparisons with the Geologic Record of Grounding Line Retreat

The Ross Sea Embayment geologic record suggests a complex pattern of asynchronous retreat over the last deglaciation. In the western Ross Sea Embayment, retreat began in the Pennell Trough (PT; Fig. 1e) at ~15 ka and in the JOIDES Trough (JT; Fig. 1e) at ~13 ka (Prothro et al., 2020). Meanwhile, in the eastern Ross Sea Embayment, small-scale retreat in Wales Deep (WD Fig. 1e) also began at ~15 ka and increased during the early Holocene (Bart et al., 2018). Across the west and east Ross Sea Embayment, the ice sheet remained grounded to the trough banks, as the ice sheet retreated through submarine troughs, forming embayments (Halberstadt et al., 2016). The grounding line then retreated throughout the Holocene (Bart et al., 2018; Halberstadt et al., 2016; Prothro et al., 2020). Prior to ~8.6 ka, ice stream flow paths changed direction, and readvanced near Drygalski Trough (DT; Figure 1e; Greenwood et al., 2018; Lee et al., 2017). It is possible that local GIA uplift played a role in this ice stream reorganization as ~60 m of uplift occurred in this region from the LGM to the early Holocene (Figure S7).

A common pattern across ice sheet histories is a decrease in zones of potential persistence within the deep submarine troughs near the edge of the continent shelf (Figure 3), which occurs due to sea-level rise driven by far-field ice-sheet melt (Supplementary Figure S4). The ridges separating the submarine troughs are shallow enough to stabilize the grounding line, despite relative sea-level rise during the deglaciation (Figure 4c), which prevents a decrease in zones of potential persistence along these ridges. In the geologic record, geomorphic features suggests that the grounding line back-steps up these banks throughout the deglaciation (Halberstadt et al., 2016). Our modeling suggests this back-stepping may be caused by sea-level rise driven by Northern Hemisphere ice sheets, which forces the grounding line to shallower depths, in addition to other drivers of retreat, such as ocean forcing.

4. Conclusion

Over the deglaciation, the Ross Sea Embayment experienced sea-level fall within its interior due to glacial isostatic rebound, and sea-level rise near the edge of the continental shelf due to far field sea-level rise, and secondarily due to peripheral bulge collapse. We use a simple model of grounding line stability to show that glacial isostatic adjustment promotes grounding line persistence near the edge of the continental shelf at the Last Glacial Maximum and near the present-day grounding line at the present-day, resulting in a net upstream migration of zones of potential persistence across the deglaciation. We also show that coarse bathymetric resolution

underpredicts grounding line persistence near the present-day grounding line and within the deep submarine troughs of the Ross Sea, thereby underestimating the impact of glacial isostatic adjustment. This finding highlights the importance of resolving small-scale bathymetric features when modeling deglacial and potential grounding line re-advance scenarios in the Holocene. In this study we have shown that, in addition to impacting transient grounding line retreat, glacial isostatic adjustment promotes stability across ice-age timescales by shifting zones of potential grounding line persistence from near the edge of the continental shelf toward the present-day grounding line across the deglaciation. Our results highlight the role of ~~topography~~bathymetry, as modulated by solid-Earth processes, in shaping the history of ice sheet advance and retreat on glacial-interglacial timescales.

5. Author contribution

Conceptualization – STK, TP, JG, ST, EP

Investigation – STK, TP, AAR, JEC, NG, CV

Formal Analysis – STK, JEC

Methodology– STK, TP, AAR, JEC, NG

Project Administration – TP, TB

Writing (original draft) – STK

Writing (review & editing) – STK, TP, AAR, NG, JEC, CV, EP, JG, ST, TB

6. Acknowledgements

We thank Pippa Whitehouse and Nicholas Golledge for sharing their ice sheet model output. We are grateful to Matt King, Niall Gandy, and one anonymous reviewer for comments that strengthened this manuscript. The authors acknowledge PALSEA, a working group of the International Union for Quaternary Sciences (INQUA) and Past Global Changes (PAGES)

7. Competing interests

The authors declare that they have no conflict of interest.

8. Data Availability

The model output used for this project can be found at the following zendo repository https://zenodo.org/records/15311008

9. References

544 Albrecht, T., Winkelmann, R., and Levermann, A.: Glacial-cycle simulations of the Antarctic Ice
545 Sheet with the Parallel Ice Sheet Model (PISM) – Part 2: Parameter ensemble analysis, The
546 Cryosphere, 14, 633–656, https://doi.org/10.5194/tc-14-633-2020, 2020.

547 Albrecht, T., Bagge, M., and Klemann, V.: Feedback mechanisms controlling Antarctic glacial-
548 cycle dynamics simulated with a coupled ice sheet–solid Earth model, The Cryosphere, 18,
549 4233–4255, https://doi.org/10.5194/tc-18-4233-2024, 2024.

550 Anderson, J. B., Conway, H., Bart, P. J., Witus, A. E., Greenwood, S. L., McKay, R. M., Hall, B.
551 L., Ackert, R. P., Licht, K., Jakobsson, M., and Stone, J. O.: Ross Sea paleo-ice sheet drainage
552 and deglacial history during and since the LGM, Quaternary Science Reviews, 100, 31–54,
553 https://doi.org/10.1016/j.quascirev.2013.08.020, 2014.

554 Balco, G., Brown, N., Nichols, K., Venturelli, R. A., Adams, J., Braddock, S., Campbell, S.,
555 Goehring, B., Johnson, J. S., Rood, D. H., Wilcken, K., Hall, B., and Woodward, J.: Reversible
556 ice sheet thinning in the Amundsen Sea Embayment during the Late Holocene, The Cryosphere,
557 17, 1787–1801, https://doi.org/10.5194/tc-17-1787-2023, 2023.

558 Bart, P. J. and Tulaczyk, S.: A significant acceleration of ice volume discharge preceded a major
559 retreat of a West Antarctic paleo-ice stream, Geology, 48, 313–317,
560 https://doi.org/10.1130/G46916.1, 2020.

561 Bart, P. J., DeCesare, M., Rosenheim, B. E., Majewski, W., and McGlannan, A.: A centuries-long
562 delay between a paleo-ice-shelf collapse and grounding-line retreat in the Whales Deep Basin,
563 eastern Ross Sea, Antarctica, Scientific Reports, 8, 1–9, https://doi.org/10.1038/s41598-018-
564 29911-8, 2018.

565 de Boer, B., Stocchi, P., and van de Wal, R. S. W.: A fully coupled 3-D ice-sheet–sea-level
566 model: algorithm and applications, Geoscientific Model Development, 7, 2141–2156,
567 https://doi.org/10.5194/gmd-7-2141-2014, 2014.

568 Bueler, E. and Brown, J.: Shallow shelf approximation as a "sliding law" in a
569 thermomechanically coupled ice sheet model, Journal of Geophysical Research: Earth Surface,
570 114, https://doi.org/10.1029/2008JF001179, 2009.

571 Buizert, C., Cuffey, K. M., Severinghaus, J. P., Baggenstos, D., Fudge, T. J., Steig, E. J., Markle,
572 B. R., Winstrup, M., Rhodes, R. H., Brook, E. J., Sowers, T. A., Clow, G. D., Cheng, H.,
573 Edwards, R. L., Sigl, M., McConnell, J. R., and Taylor, K. C.: The WAIS Divide deep ice core
574 WD2014 chronology – Part 1: Methane synchronization (68–31 ka BP) and the gas age–
575 ice age difference, Climate of the Past, 11, 153–173, https://doi.org/10.5194/cp-11-153-2015,
576 2015.

577 van Calcar, C. J., van de Wal, R. S. W., Blank, B., de Boer, B., and van der Wal, W.: Simulation
578 of a fully coupled 3D glacial isostatic adjustment – ice sheet model for the Antarctic ice sheet
579 over a glacial cycle, Geoscientific Model Development, 16, 5473–5492,
580 https://doi.org/10.5194/gmd-16-5473-2023, 2023.

581 Cavitte, M. G. P., Parrenin, F., Ritz, C., Young, D. A., Van Liefferinge, B., Blankenship, D. D.,
582 Frezzotti, M., and Roberts, J. L.: Accumulation patterns around Dome C, East Antarctica, in the
583 last 73 kyr, The Cryosphere, 12, 1401–1414, https://doi.org/10.5194/tc-12-1401-2018, 2018.

584 Clark, P. U. and Tarasov, L.: Closing the sea level budget at the Last Glacial Maximum,
585 Proceedings of the National Academy of Sciences, 111, 15861–15862,
586 https://doi.org/10.1073/pnas.1418970111, 2014.

587 Danielson, M. A. and Bart, P. J.: The staggered retreat of grounded ice in the Ross Sea,
588 Antarctica, since the Last Glacial Maximum (LGM), The Cryosphere, 18, 1125–1138,
589 https://doi.org/10.5194/tc-18-1125-2024, 2024.

590 Deschamps, P., Durand, N., Bard, E., Hamelin, B., Camoin, G., Thomas, A. L., Henderson, G.
591 M., Okuno, J., and Yokoyama, Y.: Ice-sheet collapse and sea-level rise at the Bølling warming
592 14,600 years ago, Nature, 483, 559–564, https://doi.org/10.1038/nature10902, 2012.

593 Golledge, N. R., Menviel, L., Carter, L., Fogwill, C. J., England, M. H., Cortese, G., and Levy,
594 R. H.: Antarctic contribution to meltwater pulse 1A from reduced Southern Ocean overturning,
595 Nature Communications, 5, https://doi.org/10.1038/ncomms6107, 2014.

596 Gomez, N., Pollard, D., and Mitrovica, J. X.: A 3-D coupled ice sheet – sea level model applied
597 to Antarctica through the last 40 ky, Earth and Planetary Science Letters, 384, 88–99,
598 https://doi.org/10.1016/j.epsl.2013.09.042, 2013.

599 Gomez, N., Pollard, D., and Holland, D.: Sea-level feedback lowers projections of future
600 Antarctic Ice-Sheet mass loss, Nat Commun, 6, 8798, https://doi.org/10.1038/ncomms9798,
601 2015.

602 Gomez, N., Latychev, K., and Pollard, D.: A coupled ice sheet-sea level model incorporating 3D
603 earth structure: Variations in Antarctica during the Last Deglacial Retreat, Journal of Climate, 31,
604 4041–4054, https://doi.org/10.1175/JCLI-D-17-0352.1, 2018.

605 Gomez, N., Weber, M. E., Clark, P. U., Mitrovica, J. X., and Han, H. K.: Antarctic ice dynamics
606 amplified by Northern Hemisphere sea-level forcing, Nature, 587, 600–604,
607 https://doi.org/10.1038/s41586-020-2916-2, 2020.

608 Greenwood, S. L., Simkins, L. M., Halberstadt, A. R. W., Prothro, L. O., and Anderson, J. B.:
609 Holocene reconfiguration and readvance of the East Antarctic Ice Sheet, Nat Commun, 9, 3176,
610 https://doi.org/10.1038/s41467-018-05625-3, 2018.

611 Halberstadt, A. R. W., Simkins, L. M., Greenwood, S. L., and Anderson, J. B.: Past ice-sheet
612 behaviour: retreat scenarios and changing controls in the Ross Sea, Antarctica, The Cryosphere,
613 10, 1003–1020, https://doi.org/10.5194/tc-10-1003-2016, 2016.

614 Haseloff, M. and Sergienko, O. V.: The effect of buttressing on grounding line dynamics, Journal
615 of Glaciology, 64, 417–431, https://doi.org/10.1017/jog.2018.30, 2018.

616 Houriez, L., Larour, E., Caron, L., Schlegel, N.-J., Adhikari, S., Ivins, E., Pelle, T., Seroussi, H.,
617 Darve, E., and Fischer, M.: Capturing Solid Earth and Ice Sheet Interactions: Insights from
618 Reinforced Ridges in Thwaites Glacier, https://doi.org/10.5194/egusphere-2024-4136, 24
619 January 2025.

620 Jamieson, S. S. R., Vieli, A., Livingstone, S. J., Cofaigh, C. Ó., Stokes, C., Hillenbrand, C.-D.,
621 and Dowdeswell, J. A.: Ice-stream stability on a reverse bed slope, Nature Geosci, 5, 799–802,
622 https://doi.org/10.1038/ngeo1600, 2012.

623 Johnston, P.: The effect of spatially non-uniform water loads on prediction of sea-level change,
624 Geophysical Journal International, 114, 615–634, https://doi.org/10.1111/j.1365-
625 246X.1993.tb06992.x, 1993.

626 Jones, R. S., Gudmundsson, G. H., Mackintosh, A. N., McCormack, F. S., and Whitmore, R. J.:
627 Ocean-Driven and Topography-Controlled Nonlinear Glacier Retreat During the Holocene:
628 Southwestern Ross Sea, Antarctica, Geophysical Research Letters, 48, 1–10,
629 https://doi.org/10.1029/2020GL091454, 2021.

630 Kendall, R. A., Mitrovica, J. X., and Milne, G. A.: On post-glacial sea level - II. Numerical
631 formulation and comparative results on spherically symmetric models, Geophysical Journal
632 International, 161, 679–706, https://doi.org/10.1111/j.1365-246X.2005.02553.x, 2005.

633 Kingslake, J., Scherer, R. P., Albrecht, T., Coenen, J., Powell, R. D., Reese, R., Stansell, N. D.,
634 Tulaczyk, S., Wearing, M. G., and Whitehouse, P. L.: Extensive retreat and re-advance of the
635 West Antarctic Ice Sheet during the Holocene, Nature, 558, 430–434,
636 https://doi.org/10.1038/s41586-018-0208-x, 2018.

637 Konrad, H., Sasgen, I., Pollard, D., and Klemann, V.: Potential of the solid-Earth response for
638 limiting long-term West Antarctic Ice Sheet retreat in a warming climate, Earth and Planetary
639 Science Letters, 432, 254–264, https://doi.org/10.1016/j.epsl.2015.10.008, 2015.

640 Lambeck, K., Purcell, A., Johnston, P., Nakada, M., and Yokoyama, Y.: Water-load definition in
641 the glacio-hydro-isostatic sea-level equation, Quaternary Science Reviews, 22, 309–318,
642 https://doi.org/10.1016/S0277-3791(02)00142-7, 2003.

643 Lambeck, K., Rouby, H., Purcell, A., Sun, Y., and Sambridge, M.: Sea level and global ice
644 volumes from the Last Glacial Maximum to the Holocene, Proceedings of the National Academy
645 of Sciences, 111, 15296–15303, https://doi.org/10.1073/pnas.1411762111, 2014.

646 Lee, J. I., McKay, R. M., Golledge, N. R., Yoon, H. I., Yoo, K.-C., Kim, H. J., and Hong, J. K.:
647 Widespread persistence of expanded East Antarctic glaciers in the southwest Ross Sea during the
648 last deglaciation, Geology, 45, 403–406, https://doi.org/10.1130/G38715.1, 2017.

649 Lin, Y., Hibbert, F. D., Whitehouse, P. L., Woodroffe, S. A., Purcell, A., Shennan, I., and Bradley,
650 S. L.: A reconciled solution of Meltwater Pulse 1A sources using sea-level fingerprinting, Nature
651 Communications, 12, https://doi.org/10.1038/s41467-021-21990-y, 2021.

652 Lowry, D. P., Han, H. K., Golledge, N. R., Gomez, N., Johnson, K. M., and McKay, R. M.:
653 Ocean cavity regime shift reversed West Antarctic grounding line retreat in the late Holocene,
654 Nat Commun, 15, 3176, https://doi.org/10.1038/s41467-024-47369-3, 2024.

655 McKenzie, M. A., Miller, L. E., Slawson, J. S., MacKie, E. J., and Wang, S.: Differential impact
656 of isolated topographic bumps on ice sheet flow and subglacial processes, The Cryosphere, 17,
657 2477–2486, https://doi.org/10.5194/tc-17-2477-2023, 2023.

658 Milne, G. A. and Mitrovica, J. X.: Postglacial sea-level change on a rotating Earth: first results
659 from a gravitationally self-consistent sea-level equation, Geophysical Journal International, 133,
660 1–19, https://doi.org/10.1046/j.1365-246X.1998.1331455.x, 1996.

661 Milne, G. A., Mitrovica, J. X., and Davis, J. L.: Near-field hydro-isostasy: The implementation of
662 a revised sea-level equation, Geophysical Journal International, 139, 464–482,
663 https://doi.org/10.1046/j.1365-246X.1999.00971.x, 1999.

664 Morlighem, M., Rignot, E., Binder, T., Blankenship, D., Drews, R., Eagles, G., Eisen, O.,
665 Ferraccioli, F., Forsberg, R., Fretwell, P., Goel, V., Greenbaum, J. S., Gudmundsson, H., Guo, J.,
666 Helm, V., Hofstede, C., Howat, I., Humbert, A., Jokat, W., Karlsson, N. B., Lee, W. S.,
667 Matsuoka, K., Millan, R., Mouginot, J., Paden, J., Pattyn, F., Roberts, J., Rosier, S., Ruppel, A.,
668 Seroussi, H., Smith, E. C., Steinhage, D., Sun, B., Broeke, M. R. van den, Ommen, T. D. van,
669 Wessem, M. van, and Young, D. A.: Deep glacial troughs and stabilizing ridges unveiled beneath
670 the margins of the Antarctic ice sheet, Nat. Geosci., 13, 132–137, https://doi.org/10.1038/s41561-
671 019-0510-8, 2020.

672 Neuhaus, S. U., Tulaczyk, S. M., Stansell, N. D., Coenen, J. J., Scherer, R. P., Mikucki, J. A., and
673 Powell, R. D.: Did Holocene climate changes drive West Antarctic grounding line retreat and
674 readvance?, Cryosphere, 15, 4655–4673, https://doi.org/10.5194/tc-15-4655-2021, 2021.

675 Nichols, K. A., Adams, J. R., Brown, K., Creel, R. C., McKenzie, M. A., Venturelli, R. A.,
676 Johnson, J. S., Rood, D. H., Wilcken, K., Woodward, J., and Roberts, S. J.: Direct Geologic
677 Constraints on the Timing of Late Holocene Ice Thickening in the Amundsen Sea Embayment,
678 Antarctica, Geophysical Research Letters, 51, e2024GL110350,
679 https://doi.org/10.1029/2024GL110350, 2024.

680 Nield, G. A., Whitehouse, P. L., King, M. A., and Clarke, P. J.: Glacial isostatic adjustment in
681 response to changing Late Holocene behaviour of ice streams on the Siple Coast, West
682 Antarctica, Geophysical Journal International, 205, 1–21, https://doi.org/10.1093/gji/ggv532,
683 2016.

684 Peltier, W. R., Argus, D. F., and Drummond, R.: Space geodesy constrains ice age terminal
685 deglaciation: The global ICE-6G_C (VM5a) model, Journal of Geophysical Research: Solid
686 Earth, 120, 450–487, https://doi.org/10.1002/2014JB011176, 2015.

687 Pittard, M. L., Whitehouse, P. L., Bentley, M. J., and Small, D.: An ensemble of Antarctic
688 deglacial simulations constrained by geological observations, Quaternary Science Reviews, 298,
689 107800, https://doi.org/10.1016/j.quascirev.2022.107800, 2022.

Pollard, D., Gomez, N., and Deconto, R. M.: Variations of the Antarctic Ice Sheet in a Coupled Ice Sheet-Earth-Sea Level Model: Sensitivity to Viscoelastic Earth Properties, Journal of Geophysical Research: Earth Surface, 122, 2124–2138, https://doi.org/10.1002/2017JF004371, 2017.

Prothro, L. O., Majewski, W., Yokoyama, Y., Simkins, L. M., Anderson, J. B., Yamane, M., Miyairi, Y., and Ohkouchi, N.: Timing and pathways of East Antarctic Ice Sheet retreat, Quaternary Science Reviews, 230, 106166, https://doi.org/10.1016/j.quascirev.2020.106166, 2020.

Rignot, E., Mouginot, J., and Scheuchl, B.: Ice Flow of the Antarctic Ice Sheet, Science, 333, 1427–1430, https://doi.org/10.1126/science.1208336, 2011.

Robel, A., A.: SSAsimpleM, 2021.

Robel, A. A., Roe, G. H., and Haseloff, M.: Response of Marine-Terminating Glaciers to Forcing: Time Scales, Sensitivities, Instabilities, and Stochastic Dynamics, Journal of Geophysical Research: Earth Surface, 123, 2205–2227, https://doi.org/10.1029/2018JF004709, 2018.

Robel, A. A., Pegler, S. S., Catania, G., Felikson, D., and Simkins, L. M.: Ambiguous stability of glaciers at bed peaks, Journal of Glaciology, 1–8, https://doi.org/10.1017/jog.2022.31, 2022.

Rutt, I. C., Hagdorn, M., Hulton, N. R. J., and Payne, A. J.: The Glimmer community ice sheet model, Journal of Geophysical Research: Earth Surface, 114, https://doi.org/10.1029/2008JF001015, 2009.

Schoof, C.: Ice sheet grounding line dynamics: Steady states, stability, and hysteresis, Journal of Geophysical Research: Earth Surface, 112, https://doi.org/10.1029/2006JF000664, 2007.

Schoof, C.: Marine ice sheet stability, Journal of Fluid Mechanics, 698, 62–72, https://doi.org/10.1017/jfm.2012.43, 2012.

Sergienko, O. and Haseloff, M.: 'Stable' and 'unstable' are not useful descriptions of marine ice sheets in the Earth's climate system, Journal of Glaciology, 69, 1483–1499, https://doi.org/10.1017/jog.2023.40, 2023.

Simkins, L. M., Greenwood, S. L., and Anderson, J. B.: Diagnosing ice sheet grounding line stability from landform morphology, The Cryosphere, 12, 2707–2726, https://doi.org/10.5194/tc-12-2707-2018, 2018.

Simms, A. R., Lisiecki, L., Gebbie, G., Whitehouse, P. L., and Clark, J. F.: Balancing the last glacial maximum (LGM) sea-level budget, Quaternary Science Reviews, 205, 143–153, https://doi.org/10.1016/j.quascirev.2018.12.018, 2019.

Venturelli, R. A., Siegfried, M. R., Roush, K. A., Li, W., Burnett, J., Zook, R., Fricker, H. A., Priscu, J. C., Leventer, A., and Rosenheim, B. E.: Mid-Holocene Grounding Line Retreat and

725 Readvance at Whillans Ice Stream, West Antarctica, Geophysical Research Letters, 47,
726 https://doi.org/10.1029/2020GL088476, 2020.

727 Whitehouse, P. L., Bentley, M. J., and Le Brocq, A. M.: A deglacial model for Antarctica:
728 Geological constraints and glaciological modelling as a basis for a new model of Antarctic
729 glacial isostatic adjustment, Quaternary Science Reviews, 32, 1–24,
730 https://doi.org/10.1016/j.quascirev.2011.11.016, 2012.